Vol. 642: 39–54, 2020
https://doi.org/10.3354/meps13317

MARINE ECOLOGY PROGRESS SERIES
Mar Ecol Prog Ser

Published May 28

Time-series of direct primary production and phytoplankton biomass in the southeastern Bering Sea: responses to cold and warm stanzas

Michael W. Lomas[1,*], Lisa B. Eisner[2,3], Jeanette Gann[3], Steven E. Baer[4], Calvin W. Mordy[5,6], Phyllis J. Stabeno[5]

[1]Bigelow Laboratory for Ocean Sciences, East Boothbay, ME 04544, USA
[2]NOAA Alaska Fisheries Science Center, Seattle, WA 98115, USA
[3]NOAA Alaska Fisheries Science Center, Auke Bay Laboratories, Juneau, AK 99801, USA
[4]Maine Maritime Academy, Castine, ME 04420, USA
[5]NOAA Pacific Marine Environmental Laboratory, Seattle, WA 98115, USA
[6]Joint Institute for the Study of the Atmosphere and Oceans, University of Washington, Seattle, WA 99185, USA

ABSTRACT: Sub-Arctic and Arctic regions are warming faster than nearly all other areas of the global ocean, leading to significant changes in ice quality and the duration of ice-covered periods. The impacts of this warming and sea ice variability on higher trophic levels in the Bering Sea is well documented, but the effects on lower trophic levels are less well understood. Phytoplankton biomass (as chlorophyll *a* [chl *a*]) and primary and nitrogen production measurements in the Bering Sea are presented from 2006–2016, a period that covers relatively colder (2007–2012) and warmer (2014–2016) temperature regimes. In warm spring periods, relative to cold spring periods, the frequency of subsurface chl *a* maxima increased, but with no significant differences in integrated chl *a* inventories. In contrast, cold fall periods were characterized by greater integrated chl *a* inventories than warm fall periods. Integrated net primary production (NPP) increased from the cold period (2007–2011) to the warm period (2014–2016). The difference in patterns in chl *a* and NPP resulted in higher phytoplankton growth rates during warm periods. Nitrate uptake rates increased from spring to fall during cold periods, while rates decreased from spring to fall during warm periods, suggesting changes in the balance of new versus regenerated production. While changes in phenological timing cannot be ruled out, changes in phytoplankton growth rate appear more important than changes in chl *a* biomass underlying increasing daily NPP. This distinction directly impacts our understanding of the linkages between warming temperatures and phytoplankton production and its implications in evaluating and understanding energy flow to higher trophic levels.

KEY WORDS: Bering Sea · Temperature anomaly · Primary production · Time-series · Phytoplankton · Nitrogen uptake · Chlorophyll

1. INTRODUCTION

Arctic and sub-Arctic seas (e.g. Norwegian/Greenland Seas, Labrador Sea, and Bering Sea) are characterized by high biological productivity and the seasonal presence of sea ice (Hunt & Drinkwater 2005). The Bering Sea region accounts for almost half of the annual US groundfish fishery catch (Overland & Stabeno 2004) and supports a productive benthic community (Grebmeier & Cooper 1995). In the southeastern Bering Sea shelf ecosystem, the presence or absence of seasonal sea ice is an important parameter that determines the physical and biological structure of the water column, not only in the spring, but for the

*Corresponding author: mlomas@bigelow.org

remainder of the growing season (Hunt et al. 2002, 2008, Stabeno et al. 2010, 2012b). The Bering Sea and other sub-Arctic and Arctic waters are predicted to be among those most severely affected by increases in ocean temperature, as relatively small changes in the heat content of the water column can have a disproportionately large effect on the spatial distribution and dynamics of sea ice (e.g. Sarmiento et al. 2004, Meier et al. 2005, Overpeck et al. 2005). Indeed, increases in regional temperatures have begun to affect the areal extent, concentration, and thickness of ice in both polar regions and sub-Arctic seas (IPCC 2007), and further changes in sea-ice extent due to either climate oscillations or warming will likely have significant impacts on these economically important ecosystems (e.g. Napp & Hunt 2001, Schumacher et al. 2003, Hunt et al. 2010, 2011).

From the 1970s to 1990s, there was a pattern of annual variability in water temperature deviations from the long-term mean in the southeastern Bering Sea (Stabeno et al. 2012b, 2017), which synchronized with a number of ecosystem parameters such as ice algae production, phytoplankton primary production, copepod production, and fisheries yield. Starting in ~2000, a shift in the oscillatory water temperature pattern occurred, from annual to multi-year stanzas of warm and cold periods relative to the long-term mean temperature (Stabeno et al. 2012b). For example, the years 2000–2005 were characterized by consistently positive (warm) anomalies from the long-term mean temperature, and the period 2007–2012 was characterized by consistently negative (cold) anomalies from the long-term mean (Stabeno et al. 2012b, 2017). More recently, 2014–2016 and 2018–2019 were again characterized by positive (warm) anomalies (Stabeno & Bell 2019). The extended warm period from 2000–2005 showed a decline in the numerical abundance of small copepods on the southeastern Bering Sea shelf, which continued into the cold period, yet their biomass remained relatively constant due to changes in community composition (Eisner et al. 2014). In stark contrast, the numerical abundance of large copepods was low during the warm period and increased over 4-fold, as did their biomass, into the subsequent cold period. These changes in copepod biomass rippled through higher trophic levels, as exemplified by a reduction in pollock production in warm years that recovered somewhat in cold years (Eisner & Yasumiishi 2018, Ianelli et al. 2018). The interconnected pattern of trophic interactions has been explained by the revised oscillating control hypothesis (OCH; Hunt et al. 2011). While the OCH does not explicitly include a role for sea-ice algae, the primary production associated with them is important for the ecosystem and grazers (e.g. Grebmeier et al. 2006, Gradinger 2009, Durbin & Casas 2014) and has recently been modeled to increase substantially with decreases in ice thickness (Tedesco et al. 2019). The OCH, while focused on higher trophic levels, does describe variations in the timing of phytoplankton biomass and primary production maxima between warm and cold periods. In cold years, it is hypothesized that biomass and primary production peaks occur in association with the melt-back of seasonal sea ice due to a combination of salinity stratification of the water column and sufficient solar irradiation, so there is adequate light for algal growth. In warm periods, where seasonal sea ice melts back early, it is hypothesized to result in delayed phytoplankton biomass and primary production maxima, relative to cold years, due to a lack of water column stratification and insufficient solar irradiation until later in the spring. These differences in the temporal alignment of water column stratification and incident solar irradiation have been hypothesized to impact the timing of the open-water phytoplankton production, but there is currently no hypothesized impact on the magnitude of phytoplankton biomass or rates of productivity.

Primary production measurements have been made throughout the Bering Sea shelf (e.g. Springer & McRoy 1993, Springer et al. 1996, Rho & Whitledge 2007); however, they are rarely consistent in seasonal timing and/or sampling location, making it difficult to directly assess production changes over time, although such changes have been suggested based upon impacts to other ecosystem components (e.g. Schell 2000, Hirons et al. 2001, Grebmeier et al. 2006). Mooring time series have been used to look at changes in the timing of blooms on the southeastern shelf (Sigler et al. 2014), but questions remain about converting biomass to primary production and the spatial interpolation from a single location to broader regions. Remote-sensing approaches have been employed to model primary production and thus resolve the temporal/spatial 'sampling' limitations, and have hypothesized that the loss of sea ice due to warming would increase the length of the growing season and thus annual net primary production (NPP; e.g. Loeng et al. 2005).

Without increases in nutrient recharge on the southeastern shelf, this increased NPP must be supported by enhanced internal nutrient recycling. Recent attempts to validate this hypothesis have met with mixed results; Brown et al. (2011) estimated increases in annual NPP of up to 40% with the loss of

sea ice, whereas Liu et al. (2016) suggested that differences in annual NPP are smaller, ~10%, and not significant due to the large spatial heterogeneity in the system. At least 2 environmental interactions affect the output of ocean color models used to estimate annual NPP. First is the temperature dependency of the biomass-specific maximum productivity rate (P_b^{opt}; Behrenfeld & Falkowski 1997); this is used to calculate daily NPP. Second is the interaction between stratification and vertical nutrient supply and the potential formation of subsurface chlorophyll maxima, which in turn impact the subsurface daily production profiles. The lack of a robust time-series of direct daily NPP measurements limits the ability to verify remote sensing based models of daily NPP, and thus annual NPP, associated with changes in the Bering Sea climate regime and sea ice extent.

The goal of this paper is to present data on daily rates of NPP and nitrogen (nitrate and ammonium) productivity and size-fractionated chlorophyll a (chl *a*) collected on cruises in the southeastern Bering Sea between 2006 and 2016. The dataset in total provides a nearly decade-long view of spring and fall NPP measurements during periods of colder than average temperatures (2007–2012), and warmer than average temperatures (2014–2016). We asked the following questions: (1) Are there differences in rates of NPP between the cold phase and the warm phase on the eastern Bering Sea shelf? Models suggest a minimal (10%, Liu et al. 2016) to >40% (Brown et al. 2011, Brown & Arrigo 2013) increase in annual NPP associated with warming on the Bering Sea shelf, although net community production estimates suggest that a 2-fold change in production will be required to be seen in the face of variability within the ecosystem (Lomas et al. 2012). (2) How does chl *a* size structure change between cold and warm periods, and what is the relationship to NPP? (3) How does nitrogen productivity change between cold and warm periods, and are any observed changes in concert with NPP?

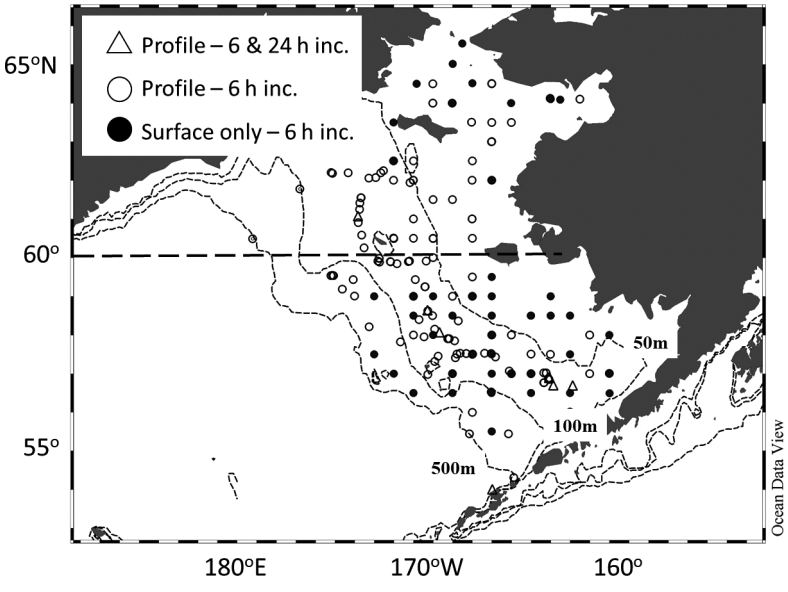

Fig. 1. All surface and profile stations compiled in this dataset. Filled circles are stations where only near-surface carbon and nitrogen productivity measurements were made; open circles are stations where a profile of 3–7 discrete samples for carbon and nitrogen productivity were measured; and open triangles are stations where paired 6 h and 24 h incubations for carbon and nitrogen productivity were conducted. Thin dashed lines are sea floor bathymetry as noted. The thick dashed line denotes the 60° N 'boundary' where changes in annual sea-ice extent are observed between warm and cold periods (Stabeno et al. 2012a)

2. MATERIALS AND METHODS

2.1. Sample collection

Samples were collected on cruises in the eastern Bering Sea as part of the Bering Arctic Subarctic Integrated Survey (BASIS), Ecosystems & Fisheries Oceanography Coordinated Investigations (EcoFOCI), and Bering Sea Ecosystem Study (BEST) programs between 2006 and 2016 (Fig. 1). While there were program-specific differences in scientific mission, all cruises collected environmental and baseline lower trophic level samples using similar protocols. For more detailed information on these programs, please see their respective websites: BEST (www.nprb.org/bering-sea-project/about-the-project), BASIS (www.fisheries.noaa.gov/alaska/population-assessments/bering-arctic-and-subarctic-integrated-survey), and EcoFOCI (www.ecofoci.noaa.gov). Detailed information on the number of stations for each cruise, incubation duration information, and whether incubations were size-fractionated is provided in Table 1. Hydrographic data were collected using a Sea-bird Electronics (SBE) 911plus or SBE 25 CTD equipped with a Wetlabs Wet-Star or ECO fluorometer with either a Licor (with log amplifier) or QSP2300 Biospherical photosynthetically active radiation (PAR) sensor (BASIS and EcoFOCI cruises), and an SBE 911plus outfitted with a Chelsea Aquatrack3 fluorometer and Biospherical QSP2300 PAR sensor (BEST cruises). CTDs and associated sensors were calibrated prior to each field year. Discrete

Table 1. Summary of metadata for each cruise included in this analysis. Environmental metrics are provided as the qualitative 'Temperature' anomaly and the average temporal sea ice coverage (% of time) during March/April which reflect the overall condition of the Bering Sea during that year. Station distribution is described by the number of stations north and south of the 60° N latitude which delineates the northern and southern shelf domains (Stabeno et al. 2012a)

Program	Cruise name	Ship	Date range	Temperature anomaly	Sea ice coverage (%)	Stations N/S of 60° N	6 h/24 h incubations	Profile stations	Stations w/size fractions
BASIS	BASIS2006		19 Aug–11 Sep 2006	Transition	6.1	3/14	17/0	0	0
BEST	HLY 07-01	USCG Healy	12 Apr–10 May 2007	Cold	6.5	4/13	0/17	17	0
BASIS	BASIS2007		25 Aug–22 Sep 2007	Cold		14/10	23/0	2	0
BEST	HLY 08-02	USCG Healy	2 Apr–1 May 2008	Cold	8.6	4/6	0/10	10	0
BASIS	BASIS2008		12–26 Sep 2008	Cold		0/11	11/0	0	0
BEST	HLY 09-02	USCG Healy	8 Apr–9 May 2009	Cold	7.5	7/11	0/18	18	0
BASIS	BASIS2009		5–13 Sep 2009	Cold		12/11	23/0	13	0
BEST	Psea 10-01	USCG Polar Sea	13–28 Mar 2010	Cold	7.7	5/0	0/5	5	0
BASIS	BASIS2010		23 Aug–4 Oct 2010	Cold		9/12	21/0	20	0
BASIS	BASIS2011		25 Aug–18 Sep 2011	Cold	6.5	1/17	13/0	18	0
EcoFOCI	DY 14-05	R/V Oscar Dyson	9–14 May 2014	Warm	4.9	0/5	4/0	4	4
EcoFOCI	DY 14-08	R/V Oscar Dyson	21–25 Sep 2014	Warm		1/4	5/0	5	1
EcoFOCI	DY 15-04	R/V Oscar Dyson	1–8 May 2015	Warm	5.1	0/6	3/3	6	1
EcoFOCI	DY 15-08	R/V Oscar Dyson	24–30 Sep 2015	Warm		1/4	5/0	5	4
EcoFOCI	DY 16-06	R/V Oscar Dyson	5–12 May 2016	Warm	5	0/6	6/0	6	0
EcoFOCI	DY 16-10	R/V Oscar Dyson	25 Sep–2 Oct 2016	Warm		0/11	9/2	11	3
				Totals		61/141	140/55	140	

water samples for rate process incubations and chl *a* measurements were generally collected at specific light depths. Based upon the PAR profile from the CTD downcast, samples were collected from depths corresponding to approximately 1.5, 3–5, 6–9, 13–17, 25–33, 50–55, and 100% of surface incident PAR (these depths were chosen to match screening in simulated *in situ* deckboard incubations). When possible, casts were conducted within several hours of local sunrise, and incubations were conducted around local solar noon. At some stations and on some cruises, primary productivity incubations were conducted on a subset of the above referenced depths.

2.2. Chlorophyll

Samples for total chl *a* analysis were collected at each depth where samples for rate process incubations were collected, and at some stations/depths, samples for size-fractionated chl *a* were also collected. Total chl *a* samples were collected by filtering a whole volume of water onto a Whatman GF/F filter (nominal pore size 0.7 µm). Size fractionation of chl *a* samples was done using slightly different protocols between cruises. On BASIS cruises in 2011 and all EcoFOCI cruises, samples were filtered sequentially through a stacked 10 µm polycarbonate filter and a Whatman GF/F filter (nominal pore size 0.7 µm) to estimate the 'large' fraction chl *a* (>5 and >10 µm) and the 'small' fraction (0.7–10 µm) chl *a*, respectively, and the 2 values were summed to yield total chl *a*. On BEST cruises, total chl *a* was sampled as previously stated, while a separate sample was filtered through a 5 µm polycarbonate filter to yield a 'large' size fraction. The 'small' fraction was calculated by difference between the 'large' fraction and total chl *a*. BASIS 2006–2010 followed the same protocol as BEST, but used a 10 µm polycarbonate filter to estimate the large size fraction. All chl *a* samples were immediately frozen (–80°C) on board ship and analyzed within 6 mo with a Turner Designs (TD-700 or 10-AU) bench top fluorometer using the acidification technique (Parsons et al. 1984) and calibrated against a commercial chl *a* standard (Sigma-Aldrich P/N 10-850).

2.3. Nutrients

Samples for nutrient analysis were collected at the same depths as chl *a* and rate process incubation samples. Samples were syringe filtered using 0.45 µm cellulose acetate membranes, and collected in 30 ml acid-washed, high-density polyethylene bottles after 3 sample rinses. On the BASIS and EcoFOCI cruises, samples were stored frozen at −80°C and analyzed later at the shore-based facility, while samples from the BEST cruises were stored at 4°C until analysis at sea, usually within 12 h of collection. Phosphate, nitrate, nitrite, and ammonium concentrations were determined using a combination of analytical components from Alpkem, Perstorp, and Technicon. World Ocean Circulation Experiment-Joint Global Ocean Fluxes Study (JGOFS) standardization and analysis procedures (Gordon et al. 1993) were closely followed, including reagent preparation, calibration of lab glassware, preparation of primary and secondary standards, and corrections for blanks and refractive index. Nutrient data from the Bering Sea program cruises were accessed from the Bering Sea Project Data Archive (Stabeno et al. 2013a,b), and data from the BASIS and EcoFOCI cruises were provided by co-author C.W.M.

2.4. Primary production incubations

Samples for primary production incubations on the BASIS and EcoFOCI cruises were comprised of profiles ranging from 3–4 (2006–2011) or 5–6 (2014–2016) light depths. For the limited profile incubations, samples were collected from every other light depth at stations during 2006–2011 (excluding 2008). For resolved profile incubations, samples were collected from 5–7 light depths (0–40 or 0–50 m) as mentioned above. For all incubations, 500 ml or 1 l clear polycarbonate incubation bottles were triple-rinsed and filled with water from the appropriate depth, and inoculated with a final concentration of 200 µM $NaH^{13}CO_3$ (99.99%). This resulted in ca. 10% atom% enrichment of the ambient carbon dioxide pool. Samples for analysis of ^{13}C natural abundance were immediately filtered onto pre-combusted (450°C, 4 h) Whatman GF/F filters. All incubation bottles were placed in screen bags simulating the light depth from which the samples were originally collected, and incubated for ca. 6 h encompassing solar noon in deck-board acrylic tanks cooled with flowing surface seawater. In most cases, incubations were terminated by filtering half of a sample onto a pre-combusted Whatman GF/F filter, representing total NPP, while the other half was sequentially filtered through a 10 µm polycarbonate filter followed by a pre-combusted Whatman GF/F filter (representing the small cell fraction). The large cell fraction was estimated by the difference between the total and the small cell fraction rates. The only exception to the above protocol was for cruises in the spring of 2014, when material was rinsed off the 10 µm polycarbonate filter and filtered onto a pre-combusted GF/F filter to measure the large cell fraction directly. In all cases, samples were frozen at −80°C until analysis.

The areal coverage of the spring EcoFOCI cruises was limited by ice in the cold period. Filling this spring data gap required inclusion of primary production incubations, and also ^{13}C incubations, conducted during the BEST program (2007–2010; downloaded from the Bering Sea Project data archive, http://data.eol.ucar.edu/; Sambrotto 2011a,b); however, these incubations were 24 h incubations as described in the US JGOFS methods manual. On EcoFOCI cruises, a small number of incubations were conducted where half of the incubation volume was filtered at ~6 h and the remaining volume filtered at ~24 h. The incubations were highly correlated (see Fig. S1 in the Supplement at www.int-res.com/articles/suppl/m642p039_supp.pdf), and clearly showed ca. 20% 'loss' of primary production during the 24 h incubation that was similar across all incubation depths. This 'loss' is in general agreement with rates of phytoplankton respiration (Tang & Peters 1995, Lefevre et al. 1997), but also likely includes some level of microzooplankton grazing loss (e.g. Sherr et al. 2013, Stoecker et al. 2014). Regardless of the specific loss process, these data are valuable to allow the intercomparison of incubations of different duration in the same region. These spring primary production data have been previously published, and details on the incubations can be found in Sambrotto et al. (2016). As described by Sambrotto et al. (2016), primary production incubations were either 24 h when nitrate concentrations were high and chl *a* concentrations were low, or ~6 h when nitrate concentrations were low and chl *a* concentrations were high. All spring NPP rates published by Sambrotto et al. (2016) are presented as daily rates.

Samples from the BASIS cruises collected from 2006–2011 were analyzed within 6 mo at the University of Alaska Fairbanks (UAF) Stable Isotope Facility using a continuous-flow isotope ratio mass spectrometry (CFIRMS) with a Delta V interfaced with a Costech ESC 4010 elemental analyzer. Quality control involved analyzing tin capsule blanks and laboratory

working standards. Blanks were analyzed every 20 samples, and working standards were analyzed every 10 samples. Twice per year, the laboratory working standards were compared to NIST standards to confirm quality assurance. Samples from the EcoFOCI cruises collected from 2014–2016 were analyzed within 6 mo at the Bigelow Laboratory Analytical Services facility on a Delta V CFIRMS integrated with a Costech 4400 elemental analyzer. The mass spectrometer was standardized on each analytical run using an 8-point mass-dependent curve using USGS40 (L-glutamic acid). The deviation in measured isotopic value from expected isotope value as a function of mass was used to correct the measured isotopic value of each sample depending upon the mass of each sample. Data from both instruments were reported in terms of atom% for each sample. All samples were corrected for natural abundance isotopic blanks comprised of filtered, but not incubated, seston collected at several stations on each cruise. Rates of primary production were calculated as in Collos & Slawyk (1985), using salinity to estimate the ambient carbon dioxide pool (Parsons et al. 1984). All NPP rates were corrected for dark carbon uptake, which was always <5% of the rate measured in the light. All rates presented herein are reported as daily rates. Rates derived from 6 h incubations were first expressed as hourly rates and then multiplied by total number of daylight hours during the day of the incubation calculated from the NOAA daylength calculator (www.esrl.noaa.gov/gmd/grad/solcalc/sunrise.html).

2.5. Nitrogen productivity incubations

Nitrogen productivity incubations were conducted as dual isotope incubations with the ^{13}C primary production incubations on the BASIS, EcoFOCI, and BEST cruises. On the BASIS and EcoFOCI cruises, nitrate and ammonium (99.99% enriched) were added to 0.1 and 0.04 µM, respectively, as there was no means to measure ambient nutrient concentrations in real time. This resulted in a median atom% enrichment of 3 and 9% for nitrate and ammonium, respectively. Incubation conditions and incubation termination were as described for primary production incubations, and rates were calculated as in Dugdale & Wilkerson (1986). Details of nitrogen incubations and rate calculations on the BEST cruises are as described by Sambrotto et al. (2016). Briefly, nitrate and ammonium daily uptake rates from the BEST cruises were calculated from hourly rates by multiplying by 12 and 18, respectively. From the remaining cruises, rates were calculated by multiplying hourly rates by the daylength as for the primary production rate calculations.

2.6. Data analysis and statistical analyses

For this manuscript, it is important to define warm and cold periods, and we used the approach of Stabeno et al. (2012b). Briefly, data from the M2 mooring (58.87° N, 164.05° W) were used to calculate a long-term mean from 1996–2016, and then individual daily temperatures were compared to the mean to determine 'warm' (positive deviations from the mean) and 'cold' periods (negative deviations from the mean). As shown by Stabeno et al. (2012b), 2001–2005 was a warm period, 2006–2012 was a cold period, and as we observed here, 2014–2016 was another warm period (Duffy-Anderson et al. 2017, Stabeno et al. 2017).

Integrations of volumetric primary production, nitrogen productivity rates, and chl *a* were conducted to 50 m, to provide consistency in integration across all profiles, using a trapezoidal integration. Where replicate samples at a given depth were measured, they were averaged prior to integration. For profiles that did not sample to a depth of 50 m, the parameter value measured at the deepest sampled depth was assumed to remain constant to a depth of 50 m. Applying this calculation approach to a subset of profiles that did sample to 50 m, suggests a potential overestimation of primary production and chl *a* by <5%, and by 5–10% for nitrogen productivity. Profiles were not corrected for any potential overestimation.

All statistical analyses were conducted using Sigma-Stat v.3.5 (Systat Software). For each analysis, normality of data distribution was always tested. When normality tests failed, non-parametric statistical tests were used rather than transforming the data. Where significant differences are referred to in the results, the specific test used is stated.

3. RESULTS

In this study, we compiled a total of 140 primary production profiles distributed over a range of cruises in cold and warm, and spring and fall periods (Table 1, Fig. 1). In addition, there are 71 stations where only 1 or 2 depths were sampled, which precludes the estimation of an integrated value at those stations; however, they do provide information on surface-only comparisons. Production measurements

were primarily made in the southeastern Bering Sea shelf (61 of the 202 stations). Equally, the dataset is more heavily skewed to sampling in the cold period, with only 38 of 201 stations sampled during the warm period, although size-fractionated NPP experiments were only conducted during the warm period. Overall, this data set allows for a meaningful direct comparison of changes in NPP in the southeastern Bering Sea between cold and warm periods over the past decade.

3.1. Chlorophyll

Profiles of chl *a* concentration at primary production stations are summarized by year and season in Fig. S1. Within a season, there was often a high degree of variability in absolute concentrations between stations, with this being most pronounced during the spring. Subsurface chl *a* maxima were observed in both in warm and cold spring and fall seasons (Table S1). In both warm and cold spring seasons, a near-benthos associated maximum was observed in 11–12% of the profiles. In contrast, a near-benthos associated maximum was observed in 38% of profiles in the cold fall and no profiles in the warm fall. In all seasons, the majority of profiles either had no vertical structure or declined with depth (Table S1). Comparison of surface chl *a* data for total and the large size classes between seasons (spring and fall) and warm and cold periods found significant differences only between warm springs and all other combinations (cold spring, cold fall, warm fall; Fig. 2A). Chl *a* concentrations measured during the warm spring period for both the total and the large size fraction were higher than concentrations in the same fraction during the cold spring period (Kruskal-Wallis 1-way ANOVA on ranks, Dunn's test for pairwise comparisons with uneven sample sizes, $p < 0.05$). Median values of total surface chl *a* were ca. 0.6–0.7 µg l^{-1} higher, roughly 2-fold, in warm spring periods than cold spring periods, although the seasonal comparison was not significant due to high variability. In addition, the large size

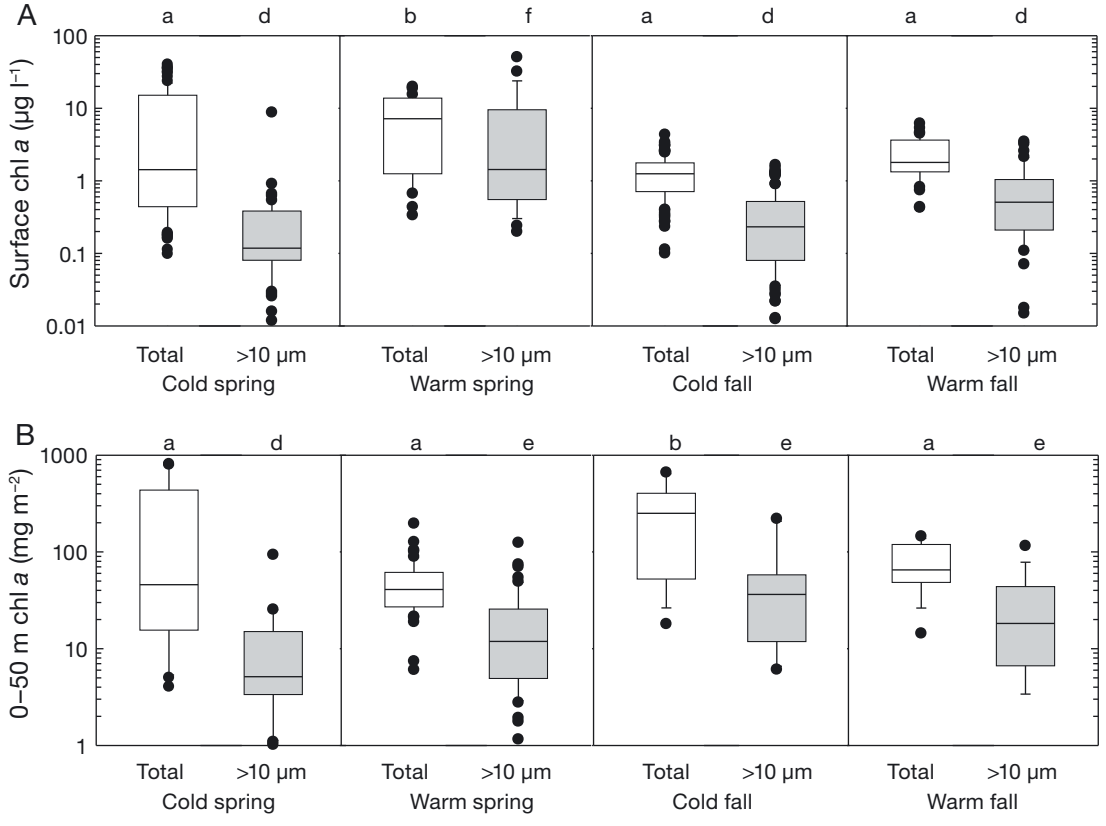

Fig. 2. Total and large size-fractioned chlorophyll (chl *a*) in (A) surface waters and (B) integrated over 0–50 m, binned by season and cold/warm period. Boundaries of the box denote the 25th and 75th percentiles, the line within the box denotes the median, whiskers denote the 10th and 90th percentiles, and data outside the 10–90th percentile range (outliers) are shown by black circles. Significant differences (Mann-Whitney rank sum test, $p < 0.05$) between seasons and cold/warm periods for total and large fractions are shown by different letters above each plot

fraction as a fraction of total chl *a* was higher in warm spring (not shown).

For the subset of stations where both chl *a* and NPP were measured, comparison of the 0–50 m integrated chl *a* concentrations for the total and large size classes between seasons and warm and cold periods also found few significant differences (Fig. 2B). Total chl *a* was significantly higher in cold fall periods than all other seasons/periods, and large size fraction chl *a* was lower in cold spring periods than all other seasons/periods (Kruskal-Wallis 1-way ANOVA on ranks, Dunn's test for pairwise comparisons with uneven sample sizes, $p < 0.05$).

3.2. NPP

Regardless of season or year, nearly all NPP profiles exhibited highest values at the surface, which decreased with light level (Fig. S2). A small percentage of the profiles showed minor (~10%) increases in rates of NPP at the deeper light depths (generally 5–30% surface irradiance), consistent with the small percentage of profiles demonstrating subsurface chl *a* maxima, suggesting that these subsurface chl *a* maxima are physiologically competent. Rates at near surface depths (50–100% light depths) were highly variable and often spanned 2 orders of magnitude from 1 to 100 mg C m^{-3} d^{-1}, but in spring, variability could reach 3 orders of magnitude (e.g. spring 2008 and 2009).

Despite the wide range in rates of NPP in the surface layer, these rates were a reasonable predictor of 0–50 m integrated NPP (Fig. 3). Data in both spring and fall were significantly (Pearson product moment correlation, $p < 0.05$) predictable from surface (100% light depth) NPP rates with similar variance explained. The slope of the relationship was greater in the fall, suggesting a deeper distribution of biomass leading to a greater rate of increase in biomass for a given surface value.

Paired comparison of hourly rates of NPP terminated after 6 and 24 h showed a highly significant (Pearson product moment correlation, $p < 0.001$) relationship over several orders of magnitude, with ~96% of the variance in 24 h rates explained by 6 h rates (Fig. S3A). The slope of the relationship was 0.79, suggesting an overall consistent 21% loss in ^{13}C isotope content of the particulate matter over the longer incubation. Comparison of individual depths confirms a depth independence of the relationship between rates calculated from 6 and 24 h incubations. A comparison of daily rates, from the 24 h incubations, with the hourly rates from the 6 h incubations, also showed a high degree of correlation (Fig. S3B). The slope of this relationship was ~11, which is similar to the overall daylength observed in the field when the incubations were conducted (12–13 h). This observation provides additional confidence in multiplying hourly rates from short-term incubations by the daylength to yield daily rates. This result also confirms the validity of combining datasets with different incubation duration once corrections for respiratory and excretion losses during each incubation are made.

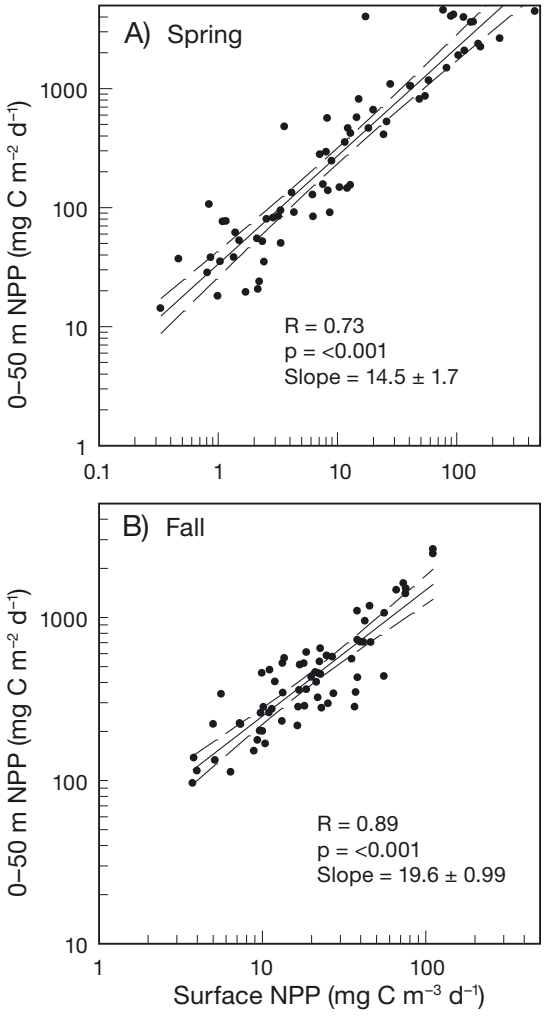

Fig. 3. Bivariate plots of 0–50 m integrated net primary production (NPP, mg C m^{-2} d^{-1}) versus surface (100% incubation irradiance) NPP (mg C m^{-3} d^{-1}) for (A) spring and (B) fall data. The solid line is the Pearson correlation and the dashed lines are the 95% confidence intervals. The information at the bottom of each panel is the description of the correlation line

Rates of NPP were initially separated by region, north and south of 60° N, but there were insufficient

stations to the north in the warm period (2014–2016) to evaluate changes over time in these broad latitudinal regions, and thus all data were pooled for all following statistical comparisons. Rates of NPP in the near-surface (<5 m) incubation depths did not significantly change, increase or decrease, with year (Fig. 4A; Model I linear regression, $p > 0.05$), although there was a slight trend to decreasing rates of NPP throughout the cold phase. In contrast, 0–50 m integrated rates of NPP showed a trend of significantly increasing rates over the entire period from 2006 to 2016 (Fig. 4B, Model 1 linear regression, $p < 0.01$), at an annual rate of 98.6 ± 35.6 mg C m^{-2} d^{-1} (mean ± SD) year-over-year, or ~20% annual increase. Of particular interest is a significant reduction in variance between stations during the warm periods, both spring and fall.

The entire dataset was parsed by season and cold/warm period to determine if there was a seasonality to the observed changes. Significant differences in 0–50 m integrated rates of NPP between cold and warm periods were found in both spring and fall, where integrated rates of NPP in warm spring periods (1758 ± 1670 mg C m^{-2} d^{-1}) were significantly greater than in cold springs (834 ± 1612 mg C m^{-2} d^{-1}; Fig. 5; Dunn's test for uneven variances, $p < 0.001$). Rates of integrated NPP in fall were also significantly different between the warm (1127 ± 978 mg C m^{-2} d^{-1}) and cold (440 ± 326 mg C m^{-2} d^{-1}) periods. Furthermore, during cold years, there was a significant seasonal increase in integrated rates of NPP from spring to fall (Dunn's test for uneven sample sizes, $p < 0.001$), but there was no significant seasonal increase from spring to fall in warm years (Dunn's test for uneven sample sizes, $p = 0.40$). Size-fractionated primary production data are only available for the warm period, and thus no warm/cold period comparison can be made to know if there are differences in size structure of primary production during the late summer period, a critical time period for secondary productivity in this system. Similar to rates of integrated NPP in the whole fraction, integrated rates of NPP in the large size fraction were not significantly different between seasons during the warm years (Student's *t*-test, $p > 0.05$).

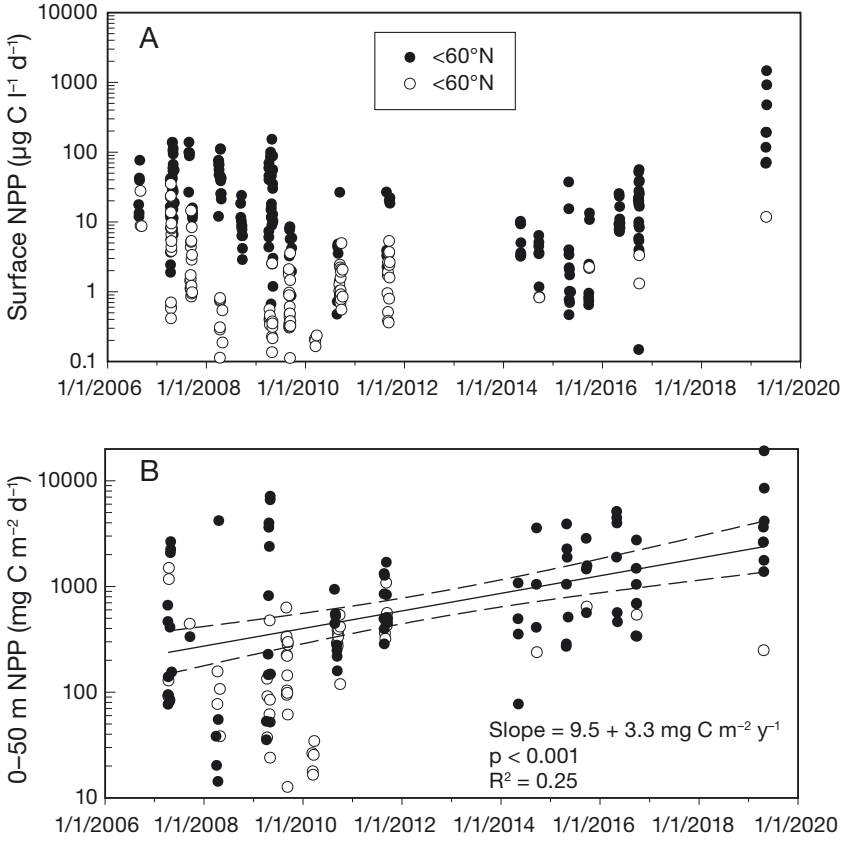

Fig. 4. (A) Surface and (B) 0–50 m integrated net primary production (NPP) as a function of time. Open symbols represent stations north of 60° N, and filled symbols represent stations south of 60° N. Model I linear regression was conducted on integrated NPP data (panel B) south of 60° N after the data were log-normal transformed to meet assumptions of normal data distribution. Regression (solid line) and 95% confidence intervals (dashed lines) are plotted, along with regression statistics

3.3. Nitrogen productivity

As with rates of NPP, nitrogen uptake rates varied widely between stations, seasons, and cold/warm years. Warm spring seasons (6.0 ± 7.3 µg N l^{-1} d^{-1}) were characterized by significantly higher surface layer NO_3^- uptake rates than cold spring seasons (1.7 ± 3.1 µg N l^{-1} d^{-1}, Student's *t*-test, $p = 0.02$). In the fall, the opposite pattern was observed, with cold fall seasons (7.5 ± 10.4 µg N l^{-1} d^{-1}) showing significantly (Student's *t*-test, $p = 0.01$) higher NO_3^- uptake rates than warm fall seasons (2.6 ± 3.8 µg N l^{-1} d^{-1}, Fig. 6A). The same patterns, including significant differences, were observed when examining 0–50 m integrated NO_3^- uptake rates (Fig. 6B).

Comparing surface uptake rates of NH_4^+, we only observed a significant difference between cold spring sea-

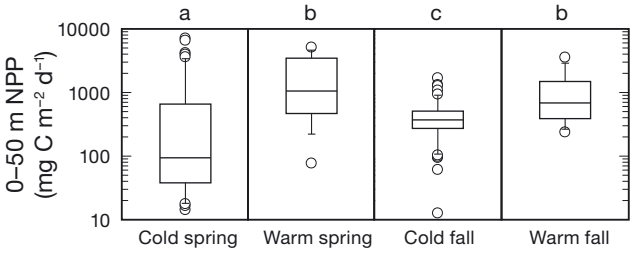

Fig. 5. Integrated (0–50 m) net primary production rates parsed by season and cold/warm period. Description of box plot parameters as in Fig. 2 (except that outliers are shown as open circles). Letters along the top of the plot denote statistically significant differences between seasons and cold/warm periods (Kruskal-Wallis 1-way ANOVA on Ranks, Dunn's test for pairwise comparisons with uneven treatment group sizes; $p < 0.05$)

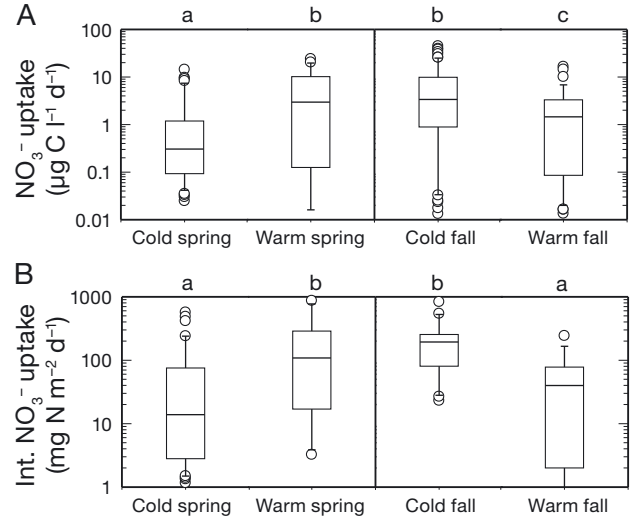

Fig. 6. (A) Surface (100% incubation light level) NO_3^- uptake rates (µg N l^{-1} d^{-1}) and (B) 0–50 m integrated NO_3^- uptake rates (mg N m^{-2} d^{-1}). In both panels, data are parsed by season and cold/warm period. Description of box plot parameters as in Fig. 5. Letters along the top of each panel denote statistically significant differences between seasons and cold/warm periods (Kruskal-Wallis 1-way ANOVA on Ranks, Dunn's test for pairwise comparisons with uneven treatment group sizes; $p < 0.05$)

sons (mean ± SD; 0.84 ± 1.26 µg N l^{-1} d^{-1}) and warm spring seasons (11.06 ± 34.44 µg N l^{-1} d^{-1}), as cold fall (14.70 ± 21.70 µg N l^{-1} d^{-1}) and warm fall (18.62 ± 27.30 µg N l^{-1} d^{-1}) seasons were not significantly different ($p = 0.38$, Student's *t*-test; data not shown). In both warm and cold periods, rates measured in the fall were significantly ($p < 0.05$, Student's *t*-test) greater than rates measured in the corresponding spring in response to higher water temperatures, but also showing the seasonally increasing importance of reduced nitrogen sources to system nitrogen metabolism. This is commonly observed, and indeed inclusion of NH_4^+ uptake rates greatly improves predictions of measured NPP in summer (Sambrotto et al. 2008). While not significantly different, warm fall NH_4^+ uptake rates were on average 30% greater than in cold fall, again showing the increased importance of regenerated nitrogen with increases in seasonal, and perhaps annual mean, temperatures. There were far fewer profiles of NH_4^+ uptake rate measurements, thus limiting statistical comparisons that could be made for integrated data. Specifically, there were only enough data for statistical comparisons during the spring season. There was no significant difference (Kruskal-Wallis 1-way ANOVA on ranks, Dunn's test; $p = 0.79$) between cold spring (25.6 ± 33.5 mg N m^{-2} d^{-1}) and warm spring (42.1 ± 47.9 mg N m^{-2} d^{-1}) NH_4^+ uptake rates. Overall, integrated NH_4^+ uptake rates were much higher in the fall; the single value in the cold fall period was 605 mg N m^{-2} d^{-1}, with a similarly high value of 405 ± 367 mg N m^{-2} d^{-1} in the warm fall period.

3.4. Carbon:nitrogen productivity ratios

To evaluate the coupling of carbon and nitrogen cycling, the ratio of integrated NPP and nitrogen uptake rates was calculated. Mean 0–50 m integrated NPP:NO_3^- uptake ratios (mol:mol) were within a factor of 3 of the Redfield ratio (6.6) for cold and warm spring periods and the cold fall period, but ~5-fold greater than the Redfield ratio in the warm fall period, showing the strong importance of NO_3^- as a nitrogen source in the Bering Sea system during colder periods (Fig. 7A). The high variance between stations/years makes a statistical evaluation of differences within this dataset difficult; however, the NPP:NO_3^- ratio in the warm fall period was significantly greater than the Redfield ratio.

Given the importance of integrated NH_4^+ uptake, this is warranted for inclusion in calculating the C:N uptake ratio. This NPP:dissolved inorganic nitrogen (DIN) calculation reduced the magnitude of the ratio closer to the Redfield ratio in all seasons and cold/warm periods where NPP:NO_3^- ratios were greater than the Redfield ratio (Fig. 7B). In fact, in the warm fall season, the inclusion of NH_4^+ uptake rates reduced the NPP:DIN ratio sufficiently that the median value was now lower than the Redfield ratio, and there was no longer a significant difference from the Redfield ratio.

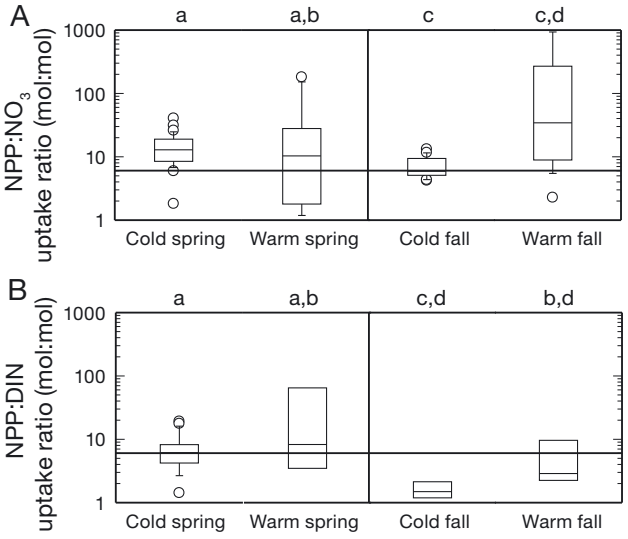

Fig. 7. 0–50 m integrated (A) net primary production (NPP):NO_3^- uptake ratios (mol:mol) and (B) NPP:dissolved inorganic nitrogen (DIN) uptake ratios (mol:mol). DIN uptake represents the sum of NO_3^- and NH_4^+ uptake rates. In both panels, data are parsed by season and cold/warm period. Description of box plot parameters as in Fig. 5. Letters along the top of each panel denote statistically significant differences between seasons and cold/warm periods (Kruskal-Wallis 1-way ANOVA on ranks, Dunn's test for pairwise comparisons with uneven treatment group sizes; $p < 0.05$). Redfield ratio indicated by solid horizontal lines

4. DISCUSSION

Given the ecological and economic importance of the southern Bering Sea, and the rapid changes it is experiencing, direct observations of phytoplankton biomass and productivity responses to climate regimes are important pieces of information to understand future responses.

4.1. Chlorophyll

While significant differences were found only for warm springs when comparing surface chl *a* values, generally warm periods were characterized by higher concentrations. This observation is consistent with previous findings based upon moorings (e.g. Stabeno et al. 2012b, 2017, Sigler et al. 2014) and ocean color algorithms (e.g. Brown et al. 2011, Liu et al. 2016). Indeed, for ocean color derived chl *a*, values at the eastern edge of the shelf break and the 'greenbelt' were up to 2 µg l^{-1} higher in the warm years which occurred at the end of the analyzed data record (2009), while other portions of the shelf and shelf break were much lower (Brown et al. 2011). The data presented here are part of a larger sampling effort over the eastern Bering Sea shelf. When examining the chl *a* dataset for 2003–2012, Eisner et al. (2016) found significantly higher chl *a* concentrations on the outer shelf and some regions in the middle domain during warm years (2003–2005), but no significant differences between thermal regimes in the northern (>63° N) Bering Sea. They found that those regions with higher total chl *a* in warm years were also characterized by a higher proportion of large-size fraction chl *a*. These elevated total chl *a* and large-size fraction chl *a* concentrations were positively associated with wind mixing and temperature, suggesting strong bottom-up controls at the time of sampling. There appears to be some debate about decreases in stratification in warm periods, due to warming of bottom waters and vertical salinity structure, that facilitates wind-induced upwelling of nutrients (e.g. Ladd & Stabeno 2012, Brown & Arrigo 2013), leaving precise mechanisms leading to enhanced chl *a* in question. A likely explanation for the lack of significant differences in our dataset is the high variance associated with the 'random' sampling of stations with bloom and non-bloom levels of chl *a* and spatial variance. These results suggest that changes in phytoplankton biomass (chl *a*) in and of themselves may not be the strongest driver of any potential changes in NPP.

4.2. NPP

The rates of NPP reported herein fall well within the range of incubation-derived spring (200–4100 mg C m^{-2} d^{-1}; McRoy et al. 1972, Whitledge 1989, Rho & Whitledge 2007, Lomas et al. 2012) and fall (500–3000 mg C m^{-2} d^{-1}; Rho & Whitledge 2007, Sambrotto et al. 2008) values reported by prior researchers. Using the remotely sensed chl *a*-based primary production algorithm (Pabi et al. 2008), Brown et al. (2011) reported climatological (1998–2007) daily rates of primary production that ranged from ~750–1250 mg C m^{-2} d^{-1} in the spring and ~500–750 mg C m^{-2} d^{-1} in the fall, generally in good agreement with direct observations. Similarly, the remotely sensed carbon-based model (Westberry et al. 2008) also yields NPP values in the range of direct incubation-based observations. Given the high spatial variability, no differences in magnitude are readily apparent between direct observations and model results.

What environmental or biological parameters are correlated with this increase in NPP from cold to warm periods? Plotting integrated NPP against

depth-weighted 0–50 m temperature for each profile showed that temperature was not a significant explanatory variable (Pearson product moment correlation; R = 0.04; p = 0.67; Fig. S4). Further, correlations with residual nitrate and DIN (nitrate + nitrite + ammonium) inventories showed no significance (Pearson product moment correlation, R < 0.02 and p > 0.9 in both instances). In fact, the only variable that was significantly correlated with integrated NPP was integrated chl *a* (Pearson product moment correlation, R = 0.56, p < 0.001). However, this correlation is driven by the broad overall range of integrated NPP values in the dataset, as average integrated chl *a* was not significantly higher for warm than cold periods, suggesting that additional environmental and/or biological (e.g. change in taxonomic composition of phytoplankton community) factors may be behind the increasing rates of NPP.

As our interest is in comparing data from cold and warm years, the data presented by Rho & Whitledge (2007) is the only other observational dataset of which we are aware that may allow a comparison of rates of NPP during a given season between cold years and warm years, although it is worth pointing out that the 'warm' period studied by Rho & Whitledge (2007) (i.e. 1980–1981; <0.5°C positive temperature anomaly) was not as anomalously warm as the 2014–2016 period (>1°C positive temperature anomaly) studied here. Rho & Whitledge (2007) found that during the spring period (April and May), rates of NPP were ~500–1500 mg C m^{-2} d^{-1} greater during the warm period studied (1979–1981) than during the cold period (1997–2000). The observed difference increased from ~500 mg C m^{-2} d^{-1} for incubations conducted on the inner shelf to 1500 mg C m^{-2} d^{-1} for incubations conducted on the middle and outer shelf. These differences represent a 50–400% increase in daily productivity estimates from cold to warm spring periods. Our observations suggest up to 100% increase in integrated rates of NPP between cold and warm spring periods, consistent with these earlier observations. Unfortunately, there is insufficient data coverage during fall in prior studies to assess differences between warm and cold fall periods. Brown et al. (2011) suggested an increase in annual NPP of 43% during the cold to warm transition that occurred from 1998–2007, although 2007 is classified as a cold year (Stabeno et al. 2012b). Using the data presented by Brown et al. (2011), we calculated that daily rates of integrated NPP increased ~33%, and thus most of the increase in annual NPP from cold to warm years is due to increased length of the growing season. It is worth noting that Brown et al. (2011) did not observe a significant increase in daily rates of NPP over time as observed in the current study. A similar modeling study by Liu et al. (2016) found the increase in daily rates of integrated gross primary production between warm years (2000–2006) and cold years (2007–2010) was only ~10%, as primary production loss rates also increased from cold years to warm years. Taken together, these prior results suggest little change in physiological growth rates and/or biomass levels between warm and cold years, with any changes in NPP driven primarily by changes in the duration of the open water growing season. In contrast, our direct observations suggest there are differences in specific carbon uptake rate (d^{-1}), a proxy for growth rate (Fig. 8). Estimated growth rates were significantly (1-way ANOVA, Dunn's test, p < 0.05) higher in warm spring periods (0.24 ± 0.20 d^{-1}) than cold spring periods (0.10 ± 0.08 d^{-1}), and warm fall periods (0.35 ± 0.27 d^{-1}) were significantly higher than cold spring and fall periods (0.14 ± 0.13 d^{-1}). The faster growth rates in warm spring versus cold spring periods is in part due to significantly higher temperatures (cold: −1.45 ± 0.87°C; warm: 2.76 ± 2.28°C), but there is also a well-recognized physiological difference in growth rate between phytoplankton taxonomic groups (Kremer et al. 2017). For example, at the same temperature, 'green' flagellates grow ~0.3 d^{-1} faster than diatoms, thus changes in taxonomic composition may also be reflected in these changes in observed growth

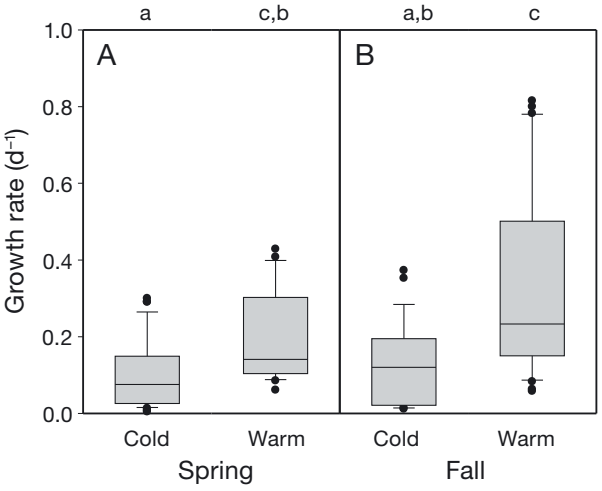

Fig. 8. Carbon-specific uptake rate as a proxy for growth rate (d^{-1}). (A) Data compiled for cold and warm spring periods, and (B) data compiled for cold and warm fall periods. Description of box plot parameters as in Fig. 2. Significant differences were determined by Kruskal-Wallis 1-way ANOVA on ranks followed by Dunn's test for pairwise comparisons with uneven treatment group sizes. Significant differences (p < 0.05) between seasons and cold/warm periods are shown by different letters

rates. Resolving biomass control and growth rate control on primary production will be important to understand future changes in NPP in this region, as well as the recognized changes in phenological timing.

4.3. Nitrogen productivity and C:N uptake ratios

Integrated NO_3^- uptake rates measured in this study, when converted to the same units, agree well with previous ranges of NO_3^- uptake rates, generally between 3 and 30 mmol m^{-2} d^{-1} but skewed to the lower end of the range, measured in the southern Bering Sea (e.g. Whitledge et al. 1986, Rho et al. 2005, Sambrotto et al. 2008, 2016). The data presented here, however, are the first of which we are aware that directly compare NO_3^- uptake rates between warm and cold periods, thus making comparison to prior observations challenging. The higher rates of NO_3^- uptake in warm spring periods are correlated with warmer mean temperatures (data not shown, Pearson product moment correlation, $p < 0.05$), which is consistent with a positive physiological temperature response (e.g. Lomas et al. 2002), although changes in NO_3^- inputs cannot be ruled out due to lack of appropriate data. Similarly, the lower NO_3^- uptake rates in warm fall periods cannot be conclusively related to NO_3^- depletion or elevated concentrations of NH_4^+ (e.g. Lomas & Glibert 1999), both of which could reduce NO_3^- uptake. However, quantifying changes in NO_3^- and NH_4^+ uptake are needed to understand the nature of primary production, new or regenerated.

Carbon to nitrogen productivity ratios can illuminate the coupling of elemental cycles. The high variance between stations/years makes a statistical evaluation of differences within this dataset difficult; however, the NPP:NO_3^- ratio in the warm fall period is significantly greater than the Redfield ratio. While NPP:NO_3^- ratios are not commonly reported in the literature, the data presented here (Fig. 7A) generally agree with the observations of Sambrotto et al. (2008), who reported NPP:NO_3^- uptake ratios of ~7–12 during the cold summer of 1981, and slightly higher values of 11–17 during the warm summer of 2004. The one exception during 2004 was at thermohaline fronts, where vertical injection of nutrients led to elevated NO_3^- uptake rates and reduced NPP:NO_3^- ratios to ~7. The inclusion of NH_4^+ uptake in calculating the C:N uptake ratio shows the potential importance of recycled nitrogen in climatologically warm seasons (e.g. Hansell et al. 1989, 1993, Varela et al. 2013), with important implications for the quantity and quality of material flow to higher trophic levels.

5. SUMMARY

The change in the thermal regime over the eastern Bering Sea shelf from annual variability to multi-year stanzas of colder and warmer than average periods has clear impacts at higher trophic levels, but the impacts at the lower trophic levels, and on productivity, are less clear. Indeed, the OCH only refers to changes in timing, not magnitudes of chl *a* or NPP. Furthermore, it is not known if the physical driver underlying this shift is a temporary change or a new normal (Stabeno et al. 2017). The warm stanza studied here (2014–2016) has been related, to varying degrees, to a greater northward flow of warm Gulf of Alaska water, periods of warm northward winds during winter, and 'residual heat' from prior years, all of which reinforce warm conditions and reduce sea ice (Stabeno et al. 2017, Stabeno & Bell 2019). These warming conditions impact water column stratification, especially in the northern Bering Sea, where salinity plays an equal role with temperature to stratify the water column (Stabeno et al. 2012a). Increases in stratification can reduce the flux of nutrients from depth, which can lead to reduced net community production and has been linked to low condition in age-0 pollock (e.g. Sambrotto et al. 1986, Mordy et al. 2012, Gann et al. 2016). However, NPP can still increase due to increases in the importance of regenerated nitrogen sources (e.g. ammonium and dissolved organic nitrogen).

This study shows that while there are differences in production between warm/cold phases for a given season, differences are not as dramatic as perhaps models have suggested (Brown et al. 2011). One explanation could be changes in the form of nitrogen supporting primary production. The importance of regenerated nitrogen sources to supporting primary production is clear; however, use of reduced nitrogen sources creates a disconnect in the foodweb between lower and higher trophic levels. While primary production supported by regenerated nitrogen may remain high, it does so by increasing growth rate/recycling rather than by increasing biomass and thus actually makes less organic material, in a net sense, for transfer to higher trophic levels. Another possible explanation for higher primary production is that when sea ice is present in March/April, an active sea-ice algae community will consume some of the nutrients from the water column (Gradinger 2009), which is rapidly exported to the benthos when the ice melts (Baumann et al. 2013), thus limiting the nutrients to be recycled in the water column later in the year. A comparison of traditional primary production meas-

urements with net community production measurements may shed some light on the variability of the southeastern Bering Sea shelf ecosystem to transfer carbon and energy to higher trophic levels, and thus support higher production at higher trophic levels. Indeed, it has been shown that late summer conditions influence lipid storage in age-0 Walleye pollock, and that this represents a critical window for energy allocation and overwinter survival to age 1 (Heintz et al. 2013, Siddon et al. 2013). Furthermore, these studies have shown that energy densities are generally lower in age-0 pollock during warm late summer periods. Further study of carbon and nitrogen productivity is warranted to understand how changes in nitrogen sources and cycling can create disconnects between phytoplankton productivity and that of higher trophic levels.

Acknowledgements. We thank the captains and crews of the R/V 'Oscar Dyson', USCG icebreakers 'Healy' and 'Polar Sea', and charter vessels 'Northwest Explorer', 'Epic Explorer', and 'Bristol Explorer', as well as the other scientists on the cruises referenced herein for their assistance and access to their data. This research was supported by NSF award ARC-1106910 and NPRB Project No. A93-03a to M.W.L. This research is contribution 5017 from the Pacific Marine Environmental Laboratory, 0934 from NOAA's Ecosystems Fisheries Oceanography Coordinated Investigations, and 2020-1054 from the Joint Institute for the Study of the Atmosphere and Ocean (JISAO), University of Washington. This publication is funded by NOAA Fisheries, NOAA Pacific Marine Environmental Laboratory, and by JISAO under NOAA Cooperative Agreement NA15OAR4320063. The research was also supported by grants from the North Pacific Research Board (517, 602, 701, 1302, and B52).

LITERATURE CITED

Baumann MS, Moran SB, Kelly RP, Lomas MW, Shull DH (2013) ^{234}Th balance and implications for seasonal particle retention in the eastern Bering Sea. Deep Sea Res II 94: 7–21

Behrenfeld MJ, Falkowski PG (1997) Photosynthetic rates derived from satellite-based chlorophyll concentration. Limnol Oceanogr 42:1–20

Brown ZW, Arrigo KR (2013) Sea ice impacts on spring bloom dynamics and net primary production in the Eastern Bering Sea. J Geophys Res Oceans 118:43–62

Brown ZW, van Dijken GL, Arrigo KR (2011) A reassessment of primary production and environmental change in the Bering Sea. J Geophys Res 116:C08014

Collos Y, Slawyk G (1985) On the compatibility of carbon uptake rates calculated from stable and radioactive isotope data: implications for the design of experimental protocols in aquatic primary productivity. J Plankton Res 7:595–603

Duffy-Anderson JT, Stabeno PJ, Siddon EC, Andrews AG and others (2017) Return of warm conditions in the southeastern Bering Sea: phytoplankton–fish. PLOS ONE 12:e0178955

Dugdale RC, Wilkerson FP (1986) The use of ^{15}N to measure nitrogen uptake in eutrophic oceans; experimental consideration. Limnol Oceanogr 31:673–689

Durbin EG, Casas MC (2014) Early reproduction by *Calanus glacialis* in the northern Bering Sea: the role of ice algae as revealed by molecular analysis. J Plankton Res 36:523–541

Eisner LB, Napp JM, Mier KL, Pinchuk AI, Andrews AGI (2014) Climate-mediated changes in zooplankton community structure for the eastern Bering Sea. Deep Sea Res II 109:157–171

Eisner LB, Yasumiishi EM (2018) Large copepod abundance (observed and modeled) as an indicator of pollock recruitment to age-3 in the southeastern Bering Sea. In: Zador S, Siddon EC (eds) Ecosystem considerations: 2018 status of the eastern Bering Sea marine ecosystem. Alaska Fisheries Science Center, Seattle, WA

Eisner LB, Gann JC, Ladd C, Cieciel KD, Mordy CW (2016) Late summer/early fall phytoplankton biomass (chlorophyll *a*) in the eastern Bering Sea: spatial and temporal variations and factors affecting chlorophyll *a* concentrations. Deep Sea Res II 134:100–114

Gann JC, Eisner LB, Porter S, Watson JT and others (2016) Possible mechanism linking ocean conditions to low body weight and poor recruitment of age-0 walleye pollock (*Gadus chalcogrammus*) in the southeast Bering Sea during 2007. Deep Sea Res II 134:115–127

Gordon L, Jennings J Jr, Ross A, Krest J (1993) A suggested protocol for continuous flow automated analysis of seawater nutrients (phosphate, nitrate, nitrite, and silicic acid) in the WOCE Hydrographic Program and the Joint Global Ocean Fluxes Study. Oregon State University, Corvallis, OR

Gradinger R (2009) Sea-ice algae: major contributors to primary production and algal biomass in the Chukchi and Beaufort Seas during May/June 2002. Deep Sea Res II 56:1201–1212

Grebmeier JM, Cooper LW (1995) Influence of the St-Lawrence-Island Polynya upon the Bering Sea benthos. J Geophys Res Oceans 100:4439–4460

Grebmeier JM, Overland JE, Moore SE, Farley EV and others (2006) A major ecosystem shift in the Northern Bering Sea. Science 311:1461–1464

Hansell DA, Goering JJ, Walsh JJ, McRoy CP, Coachman LK, Whitledge TE (1989) Summer phytoplankton production and transport along the shelf break in the Bering Sea. Cont Shelf Res 9:1085–1104

Hansell DA, Whitledge TE, Goering JJ (1993) Patterns of nitrate utilization and new production over the Bering Chukchi Shelf. Cont Shelf Res 13:601–627

Heintz RA, Siddon EC, Farley EV, Napp JM (2013) Correlation between recruitment and fall condition of age-0 pollock (*Theragra chalcogramma*) from the eastern Bering Sea under varying climate conditions. Deep Sea Res II 94:150–156

Hirons AC, Schell DM, Finney BP (2001) Temporal records of δ^{13}C and δ^{15}N in North Pacific pinnipeds: inferences regarding environmental change and diet. Oecologia 129:591–601

Hunt GL Jr, Drinkwater K (2005) GLOBEC symposium on climate variability and sub-Arctic marine ecosystems. GLOBEC Newsl 11:14

Hunt GL Jr, Stabeno P, Walters G, Sinclair E, Brodeur RD, Napp JM, Bond NA (2002) Climate change and control of the southeastern Bering Sea pelagic ecosystem. Deep Sea Res II 49:5821–5853

Hunt GL Jr, Stabeno PJ, Strom S, Napp JM (2008) Patterns of spatial and temporal variation in the marine ecosystem of the southeastern Bering Sea, with special reference to the Pribilof Domain. Deep Sea Res II 55:1919–1944

Hunt GL Jr, Bond N, Stabeno P, Ladd C and others (2010) Status and trends of the Bering Sea region, 2003–2008. In: McKinnell SM, Dagg MJ (eds) Marine ecosystems of the North Pacific Ocean; status and trends, 2003–2008. PICES Spec Publ 4, p 196–267

Hunt GL Jr, Coyle KO, Eisner LB, Farley EV and others (2011) Climate impacts on eastern Bering Sea food webs: a synthesis of new data and an assessment of the Oscillating Control Hypothesis. ICES J Mar Sci 68: 1230–1243

Ianelli JN, Kotwicki S, Honkalehto T, McCarthy A and others (2018) Assessment of walleye pollock stock in the Eastern Bering Sea. Stock Assessment and Fishery Evaluation Report for the Groundfish Resources of the Bering Sea/Aleutian Islands Regions. North Pacific Fisheries Management Council, Anchorage, AK

IPCC (2007) Climate change 2007 — impacts, adaptation and vulnerability. Working Group II contribution to the Fourth Assessment Report of the IPCC. Cambridge University Press, London

Kremer CT, Thomas MK, Litchman E (2017) Temperature- and size-scaling of phytoplankton population growth rates: reconciling the Eppley curve and the metabolic theory of ecology. Limnol Oceanogr 62:1658–1670

Ladd C, Stabeno PJ (2012) Stratification on the Eastern Bering Sea shelf revisited. Deep Sea Res II 65–70: 72–83

Lefevre D, Minas HJ, Minas M, Robinson C, Williams PJL, Woodward EMS (1997) Review of gross community production, primary production, net community production and dark community respiration in the Gulf of Lions. Deep Sea Res II 44:801–832

Liu CL, Zhai L, Zeeman SI, Eisner LB and others (2016) Seasonal and geographic variations in modeled primary production and phytoplankton losses from the mixed layer between warm years and cold years on the eastern Bering Sea shelf. Deep Sea Res II 134:141–154

Loeng H, Brader K, Carmack EC, Denisenko S and others (2005) Marine systems. Arctic climate impact assessment. Cambridge University Press, Cambridge

Lomas M, Glibert P (1999) Interactions between NH_4^+ and NO_3^- uptake and assimilation: comparisons of diatoms and dinoflagellates at several growth temperatures. Mar Biol 133:541–551

Lomas MW, Glibert PM, Shiah FK, Smith EA (2002) Microbial processes and temperature in Chesapeake Bay: current relationships and potential impacts of regional warming. Glob Change Biol 8:51–70

Lomas MW, Moran SB, Casey JR, Bell DW and others (2012) Spatial and seasonal variability of primary production on the Eastern Bering Sea shelf. Deep Sea Res II 65–70: 126–140

McRoy CP, Goering JJ, Shiels W (1972) Studies of primary production in the eastern Bering Sea. In: Takenouti A (ed) Biological oceanography of the northern north Pacific Ocean. Idemitsu Shoten, Tokyo, p 199–216

Meier W, Stroeve J, Fetterer F, Knowles K (2005) Reductions in Arctic sea ice cover no longer limited to summer. EOS Trans Am Geophys Union 86:325–326

Mordy C, Cokelet ED, Ladd C, Menzia F, Proctor P, Stabeno PJ, Wisegarver E (2012) Net community production on the middle shelf of the eastern Bering Sea. Deep Sea Res II 65-70:110–125

Napp JM, Hunt GJ Jr (2001) Anomalous conditions in the south-eastern Bering Sea 1997: linkages among climate, weather, ocean, and biology. Fish Oceanogr 10: 61–68

Overland JE, Stabeno P (2004) Is the climate of the Bering Sea warming and impacting the ecosystem? EOS Trans Am Geophys Union 85:309–310, 312

Overpeck JT, Sturm M, Francis JA, Perovich DK and others (2005) Arctic system on trajectory to new, seasonally ice-free state. EOS Trans Am Geophys Union 86: 309–313

Pabi S, van Dijken GL, Arrigo KR (2008) Primary production in the Arctic Ocean. J Geophys Res 113:C08005

Parsons TR, Maita Y, Lalli CM (1984) A manual of chemical and biological methods for seawater analysis. Pergamon Press, New York, NY

Rho TK, Whitledge TE (2007) Characteristics of seasonal and spatial variations of primary production over the southeastern Bering Sea shelf. Cont Shelf Res 27: 2556–2569

Rho TK, Whitledge TE, Goering JJ (2005) Interannual variations of nutrients and primary production over the southeastern Bering Sea shelf during the spring of 1997, 1998, and 1999. Oceanology 45:376–390

Sambrotto R (2011a) Nitrogen and carbon uptake rates (on-deck) and particulate carbon and nitrogen data. Version 1.0. UCAR/NCAR - Earth Observing Laboratory. https://doi.org/10.5065/D67W696R

Sambrotto R (2011b) PSEA-10-01 Nitrate and carbon uptake rates (in-situ) and particulate carbon and nitrogen data. Version 1.0. UCAR/NCAR - Earth Observing Laboratory. https://doi.org/10.5065/D6DN4339

Sambrotto R, Niebauer HJ, Goering JJ, Iverson RL (1986) Relationships among vertical mixing, nitrate uptake, and phytoplankton growth during the spring bloom in the southeast Bering Sea middle shelf. Cont Shelf Res 5: 161–198

Sambrotto RN, Mordy CW, Zeeman SI, Stabeno PJ, Macklin SA (2008) Physical forcing and nutrient conditions associated with patterns of Chl *a* and phytoplankton productivity in the southeastern Bering Sea during summer. Deep Sea Res II 55:1745–1760

Sambrotto RN, Burdloff D, Mckee KT (2016) Spatial and year-to-year patterns in new and primary productivity in sea ice melt regions of the eastern Bering Sea. Deep Sea Res II 134:86–99

Sarmiento JL, Slater R, Barber R, Bopp L and others (2004) Response of ocean ecosystems to climate warming. Glob Biogeochem Cycles 18:GB3003

Schell DM (2000) Declining carrying capacity in the Bering Sea: isotopic evidence from whale beleen. Limnol Oceanogr 45:459–462

Schumacher JD, Bond NA, Brodeur RD, Livingston P, Napp JM, Stabeno PJ (2003) Climate change in the southeastern Bering Sea and some consequences for biota. In: Hempel G, Sherman K (eds) Large marine ecosystems of the world: trends in exploitation, protection, and research. Elsevier, Amsterdam, p 17–40

Sherr EB, Sherr BF, Ross C (2013) Microzooplankton grazing impact in the Bering Sea during spring sea ice conditions. Deep Sea Res II 94:57–67

Siddon EC, Kristiansen T, Mueter FJ, Holsman KK, Heintz RA, Farley EV (2013) Spatial match-mismatch between

juvenile fish and prey provides a mechanism for recruitment variability across contrasting climate conditions in the eastern Bering Sea. PLOS ONE 8:e84526

Sigler MF, Stabeno PJ, Eisner LB, Napp JM, Mueter FJ (2014) Spring and fall phytoplankton blooms in a productive subarctic ecosystem, the eastern Bering Sea, during 1995–2011. Deep Sea Res II 109:71–83

Springer AM, McRoy CP (1993) The paradox of pelagic food webs in the northern Bering Sea. III. Patterns of primary production. Cont Shelf Res 13:575–599

Springer AM, McRoy CP, Flint MV (1996) The Bering Sea Green Belt: shelf-edge processes and ecosystem production. Fish Oceanogr 5:205–233

Stabeno PJ, Bell SW (2019) Extreme conditions in the Bering Sea (2017–2018): record breaking low sea-ice extent. Geophys Res Lett 46:8952–8959

Stabeno PJ, Napp JM, Mordy CW, Whitledge T (2010) Factors influencing physical structure and lower trophic levels of the eastern Bering Sea shelf in 2005: sea ice, tides and winds. Prog Oceanogr 85:180–196

Stabeno PJ, Farley EV Jr, Kachel NB, Moore S and others (2012a) A comparison of the northern and southern shelves of the eastern Bering Sea and some implications for the ecosystem. Deep Sea Res II 65–70:14–30

Stabeno PJ, Kachel NB, Moore SE, Napp JM, Sigler M, Yamaguchi A, Zerbini AN (2012b) Comparison of warm and cold years on the southeastern Bering Sea shelf and some implications for the ecosystem. Deep Sea Res II 65–70:31–45

Stabeno P, Sonnerup R, Mordy C, Whitledge T (2013a) HLY-08-02 CTD and nutrient data. Version 4.0. UCAR/NCAR - Earth Observing Laboratory. https://doi.org/10.5065/D60K26KN

Stabeno P, Sonnerup R, Mordy C, Whitledge T (2013b) HLY-09-02 CTD and nutrient data. Version 3.0. UCAR/NCAR - Earth Observing Laboratory. https://doi.org/10.5065/D6SB43R4

Stabeno PJ, Duffy-Anderson JT, Eisner LB, Farley EV, Heintz RA, Mordy CW (2017) Return of warm conditions in the southeastern Bering Sea: physics to fluorescence. PLOS ONE 12:e0185464

Stoecker DK, Weigel A, Goes JI (2014) Microzooplankton grazing in the Eastern Bering Sea in summer. Deep Sea Res II 109:145–156

Tang EPY, Peters R (1995) The allometry of algal respiration. J Plankton Res 17:303–315

Tedesco L, Vichi M, Scoccimarro E (2019) Sea-ice algal phenology in a warmer Arctic. Sci Adv 5:eaav4830

Varela DE, Crawford DW, Wrohan IA, Wyatt SN, Carmack EC (2013) Pelagic primary productivity and upper ocean nutrient dynamics across subarctic and arctic seas. J Geophys Res Oceans 118:7132–7152

Westberry T, Behrenfeld MJ, Siegel DA, Boss E (2008) Carbon-based primary productivity modeling with vertically resolved photoacclimation. Glob Biogeochem Cycles 22: GB2024

Whitledge TE (1989) Carbon and nitrogen cycling within the Bering and Chukchi Seas. Prog Oceanogr 22: 279–361

Whitledge TE, Reeburgh WS, Walsh JJ (1986) Seasonal inorganic nitrogen distributions and dynamics in the southeastern Bering Sea. Cont Shelf Res 5:109–132

Editorial responsibility: Steven Lohrenz, New Bedford, Massachusetts, USA

Submitted: November 2, 2019; Accepted: March 31, 2020
Proofs received from author(s): May 15, 2020